Aerospace Systems
https://doi.org/10.1007/s42401-023-00268-9

ORIGINAL PAPER

Hysteresis of oscillatory airflow in a supersonic intake model

Alexander Kuzmin[1]

Received: 22 October 2023 / Revised: 2 December 2023 / Accepted: 9 December 2023

Abstract
Supersonic airflow deceleration in a conventional mixed-compression intake is studied numerically. The simulation of turbulent two-dimensional flow is based on the Reynolds-averaged Navier–Stokes equations and the k-ω SST turbulence model. Numerical solutions are obtained with ANSYS-18.2 CFX finite-volume solver of second-order accuracy. The solutions reveal flow hysteresis with step-by-step changes in the free-stream Mach number M_∞. The hysteresis is caused by the instability of an interaction of a shock wave with the local region of flow acceleration formed near the throat of intake. Oscillations of the Mach number M_∞ in time are considered as well, and the existence of hysteresis is confirmed at small values of the amplitude A and period τ of the oscillations. The hysteresis shrinks with increasing amplitude A and eventually disappears at sufficiently large amplitudes. The dependence of shock wave oscillations on the period τ is also studied and transitions between different flow regimes are discussed.

Keywords Turbulent flow · Numerical simulation · Shock waves · Oscillations · Hysteresis

1 Introduction

The efficiency of an air-breathing engine designed for a supersonic vehicle depends substantionally on the intake that decelerates the incoming atmospheric airflow to velocities suitable for fuel burning in the combustor. In on-design conditions, the deceleration and compression of supersonic flow are accomplished through several oblique shock waves generated by ramps and cowl of the mixed compression intake. Such a flow regime is known as started intake [1, 2]. If the free-stream Mach number M_∞ drops below the on-design value or the pressure imposed at the exit p_{exit} increases, then the shock system shifts upstream and eventually is expelled from the intake. This regime is known as unstarted intake with a nearly normal shock ahead of entrance, resulting in considerable losses in the total pressure. The intake can be restarted again by increasing M_∞ or decreasing p_{exit} if the contraction ratio (i.e., the ratio of the cross-sectional area at the entrance to the throat area) is not large.

The unstart and start of an intake are usually accompanied by hysteresis. For a convergent-divergent Busemann biplane at zero angle of attack, two-dimensional numerical simulations showed the existence of flow hysteresis with a variation of M_∞ in the band $1.64 \le M_\infty \le 2.18$ [3]. Subsequent experiments confirmed the hysteresis [4], although they demonstrated some discrepancy with numerical results owing to 3D effects.

Guo et al. [5] and Li [6] numerically and experimentally explored supersonic flow deceleration in a curved channel. The existence of flow hysteresis with changes in the backpressure p_{exit} was demonstrated. Two causes of this phenomenon were identified: the initial pressure distribution and self-sustaining characteristics of a separation region.

Feng et al. [7, 8] performed experimental and numerical investigations of the airflow in a dual-mode combustor at $M_\infty = 3$. A pressure hysteresis on a wall of the channel under variation of the exit area was demonstrated.

For a typical convergent-divergent intake, Das and Prasad [9] studied the effects of cowl deflection angles and changes in the backpressure p_{exit} at $M_\infty = 2.2$. It was shown that a small cowl deflection angle can produce a noticeable improvement in the aerodynamic performance of the intake. The improvement was compared with that achieved by a conventional technique of bleeding through suitable holes in the vicinity of the intake throat.

Jin et al. [10] focused on a numerical and experimental study of flow hysteresis in a convergent-divergent intake with

✉ Alexander Kuzmin
a.kuzmin@spbu.ru

[1] Department of Fluid Dynamics, St. Petersburg State University, St. Petersburg, Russia

Published online: 13 January 2024

variable geometry of the throat. Flow separation ahead of intake was identified as a major factor influencing hysteresis.

A number of works have addressed flow nonuniqueness and hysteresis in hypersonic intakes [11, 12]. In particular, the interaction of the external compression shock and boundary layer on the cowl was shown to play a key role in the hysteresis phenomenon.

Kuzmin [13, 14] focused on supersonic flow deceleration in 9°-bent channels of constant cross-section areas before and after the bend. Special attention was given to the interaction of a shock wave reflected from the cowl tip with an expansion flow region over the convex wall of the channel. Instability of the interaction was shown to cause a hysteresis of shock location with changes in Mach number M_∞ or backpressure p_{exit}. In addition, computations revealed a double hysteresis (with three branches of the hysteresis curve) in narrow bands of M_∞ or p_{exit}.

A subsequent paper [15] was concerned with oscillatory flows in 9°-bent channels at Mach numbers ranging from 1.56 to 1.63. Transitions between different regimes under forced oscillations of the Mach number $M_\infty(t)$ or backpressure p_{exit}(t) were examined. It was shown that hysteresis in a long channel is essentially wider than that in a short channel.

In the present paper, we perform a similar study of oscillatory flow in a mixed compression intake treated by Das and Prasad [9]. In Sect. 2, we formulate the problem and outline a numerical method. Then, in Sect. 3, we demonstrate flow hysteresis with a step-by-step variation in the steady Mach number in the band $1.9 \le M_\infty \le 2.2$. Section 4 addresses flow behavior under forced harmonic oscillations of M_∞. Transitions between different flow regimes with changes in the midvalue, amplitude, or period of the Mach number are discussed, and the existence of flow hysteresis is confirmed.

2 Problem formulation and numerical method

Figure 1 shows the intake geometry and outer boundaries of the computational domain, where the Cartesian coordinates (x,y) are dimensional and given in millimeters. The total length of the lower wall is 119 mm. The first and second ramps of the wall are 7° and 14°, respectively. Coordinates of the cowl tip are $x = 22.98$ mm, $y = 15$ mm. The inner and outer surfaces of the cowl make angles of 4° and 7°, respectively, with the freestream that is parallel to the x-axis. The height of the intake at the exit is 12 mm. More details of the intake geometry are available in [9].

The air is treated as a perfect gas whose molar mass is 28.96 kg/kmol, the ratio of specific heats is 1.4, and the specific heat at constant pressure is 1004.4 J/(kg K). For the molecular dynamic viscosity, we use the Sutherland formula.

On the inflow boundary of the computational domain, we set the x- and y-components of flow velocity $U_\infty = M_\infty a_\infty$, $V_\infty = 0$, turbulence level of 0.5%, static pressure $p_\infty = 4.47 \times 10^4$ N/m^2, and static temperature $T_\infty = 161$ K, which determines the sound speed $a_\infty = 254.4$ m/s. The chosen parameters correspond to those in a test section of the wind tunnel used for experiments in [9]. The Reynolds number based on $M_\infty = 2.0$ and the height $h = 15$ mm of the cowl tip is 6.7×10^5.

The condition of supersonic flow $M(x,y) > 1$ is prescribed at the exit of intake and on the outflow boundary of the computational domain over the cowl. The vanishing heat flux and no-slip condition are imposed on the walls. Initial data are determined by the free stream or a flow field obtained for other values of M_∞.

The initial-boundary value problem was solved with ANSYS-18.2 CFX finite-volume solver [16] based on the system of unsteady Reynolds-averaged Navier–Stokes equations with respect to static pressure $p(x,y,t)$, temperature $T(x,y,t)$, and velocity components $U(x,y,t)$, $V(x,y,t)$ [17]. We used a high-resolution numerical scheme for convective terms and an implicit backward Euler scheme for advancing in time t. A Shear Stress Transport k-ω turbulence model by Menter [18] was employed for the calculation of Reynolds stresses.

Computations were performed on an unstructured mesh consisting of quadrilaterals in 40 layers on the wall and cowl of intake, and by triangles in the remaining region. The nondimensional thickness y^+ of the first mesh layer was less than 1.2. The total number of mesh cells was 612,127. Test computations on a refined grid of approximately 1.3×10^9 cells only showed insignificant changes (< 1.3%) in shock wave coordinates. A global timestep of 5×10^{-7} s ensured that the root-mean-square Courant–Friedrichs–Lewy number was smaller than 4. At $M_\infty = 2.2$, the calculated shock system demonstrated good agreement with the numerical and experimental results provided for this particular case by Das and Prasad (see a comparison in [19]).

3 Results and discussion

3.1 Steady free-stream Mach number M_∞

At given steady values of M_∞, transient solutions of the initial-boundary value problem demonstrated a fast convergence of the mean parameters of turbulent flow to steady states. The states turned out to be nonunique in a narrow band of M_∞. For example, to demonstrate the nonuniqueness at $M_\infty = 2.04$, one can solve the problem at $M_\infty = 1.9$ and $M_\infty = 2.2$, and then use the obtained flow fields as initial data for solving the problem at $M_\infty = 2.04$. In this way, computations produced two different flows, as depicted in Fig. 1a

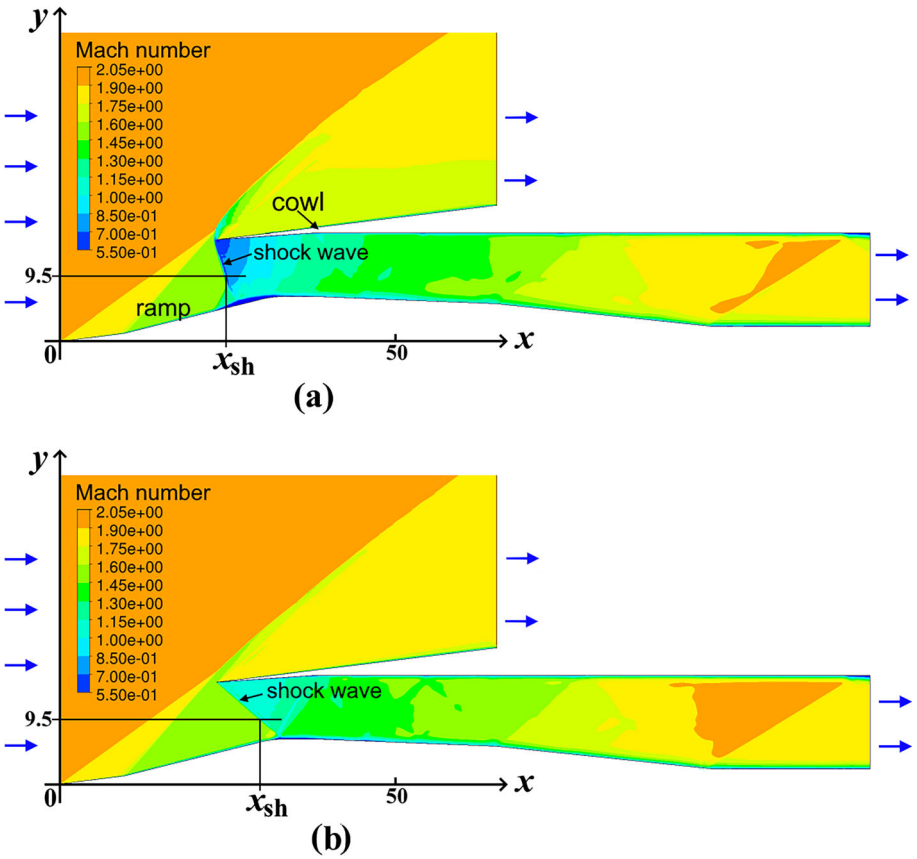

Fig. 1 Mach number contours at $M_\infty = 2.04$ in two different regimes, in which the shock wave is **a** nearly normal and located at the entrance, **b** oblique and attaining the top of the lower wall/throat of the intake

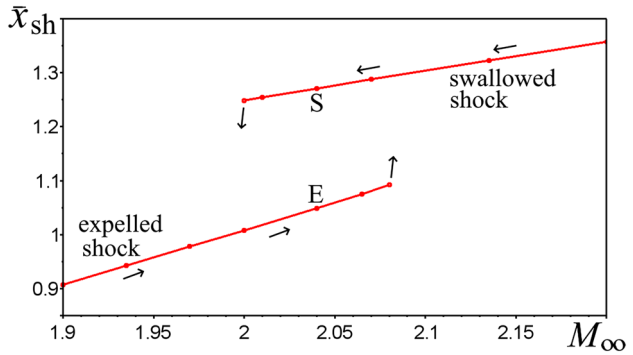

Fig. 2 The coordinate $\bar{x}_{sh}$ of shock wave as a function of the steady Mach number M_∞

and b. Figure 1a shows that the shock formed at the entrance is nearly normal, whereas in Fig. 1b the shock is oblique and attains the top of the lower wall (throat of intake).

The longitudinal location of a shock wave can be traced, e.g., with its x-coordinate x_{sh} at the height $y = 9.5$ mm, as shown in Fig. 1. In what follows, we will use the non-dimensional quantity $\bar{x}_{sh} = x_{sh}/22.98$ mm (that is the ratio of x_{sh} to the x-coordinate of the cowl tip). Calculated values of $\bar{x}_{sh}$ with step-by-step changes in M_∞ are depicted in Fig. 2. The lower branch of the curve corresponds to the flow regime in which the shock is nearly normal and resides in the vicinity of the entrance (expelled shock). The upper branch corresponds to the flow regime with an oblique shock attaining the throat (swallowed shock). Evidently, there is hysteresis in the band $2.00 \le M_\infty \le 2.03$, which corresponds to changes in the free-stream velocity U_∞ from 508.8 to 516.4 m/s.

3.2 Dependence of shock location on the amplitude *A* of Mach number oscillations

To study oscillatory regimes in the intake, we impose the free-stream Mach number as follows:

$$M_\infty(t) = M_{mid} + A\sin(2\pi t/\tau), \quad (1)$$

where t is time and τ is the period of oscillations. This incurs forced oscillations of the shock wave. For instance, at $M_{mid} = 2.04$, $A = 0.04$, $\tau = 0.02$ s and initial steady state with an expelled shock (point E in Fig. 2), the dependence of the coordinate $\bar{x}_{sh}$ on time is illustrated by curve 2 in Fig. 3. As seen, $\bar{x}_{sh}(t)$ does not exceed 1.09; therefore, the initial flow regime with the expelled shock persists.

For the initial state with a swallowed shock (point S in Fig. 2) and the same $M_{mid} = 2.04$, $A = 0.04$, $\tau = 0.02$, a dependence of $\bar{x}_{sh}$ on time is illustrated by curve 2 in Fig. 4.

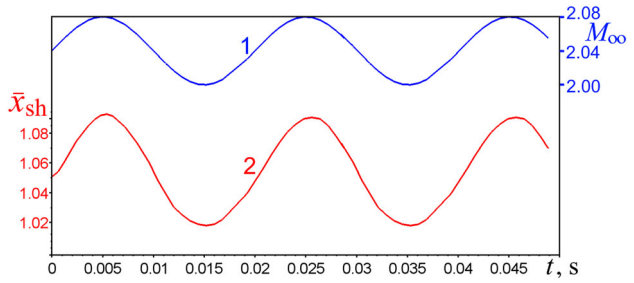

Fig. 3 1—given oscillations (1) of M_∞ in time t; 2—calculated shock coordinate $\bar{x}_{sh}$ at $M_{mid} = 2.04$, $\tau = 0.02$ s, $A = 0.04$ and initial state with an expelled shock

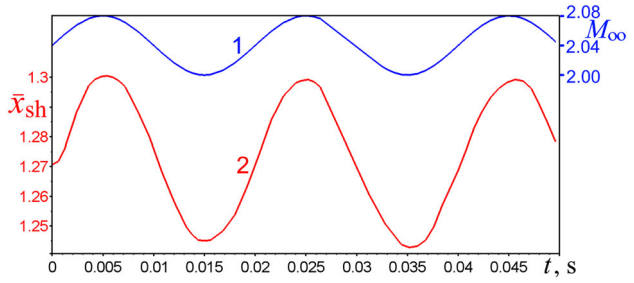

Fig. 4 1—given oscillations (1) of M_∞ in time t; 2—calculated shock coordinate $\bar{x}_{sh}$ at $M_{mid} = 2.04$, $\tau = 0.02$ s, $A = 0.04$ and initial state with a swallowed shock

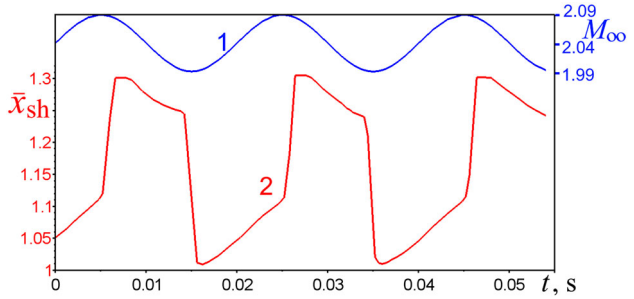

Fig. 5 1—given oscillations of M_∞; 2—calculated shock coordinate $\bar{x}_{sh}$ at $M_{mid} = 2.04$, $\tau = 0.02$ s, $A = 0.05$ and initial state with an expelled shock

As seen, $\bar{x}_{sh}(t)$ oscillates between $\bar{x}_{sh,min} = 1.24$ and $\bar{x}_{sh,max} = 1.30$; therefore, the initial flow regime again persists.

A rise of the amplitude A from 0.04 to 0.05 under retained $M_{mid} = 2.04$, $\tau = 0.02$ s enhances the shock oscillations in such a way that $\bar{x}_{sh}(t)$ turns out to alternate between 1.01 and 1.30, i.e., between vicinities of the entrance and throat of intake, see Figs. 5 and 6.

3.3 Dependence of shock location on the period τ and midvalue M_{mid} of Mach number oscillations

An increase in τ from 0.02 to 0.06 at $M_{mid} = 2.04$, $A = 0.04$ in the case of an initial state with a swallowed shock (point S in Fig. 2) triggers a transition to the regime with an expelled shock in which $\bar{x}_{sh}(t) < 1.09$, see Fig. 7.

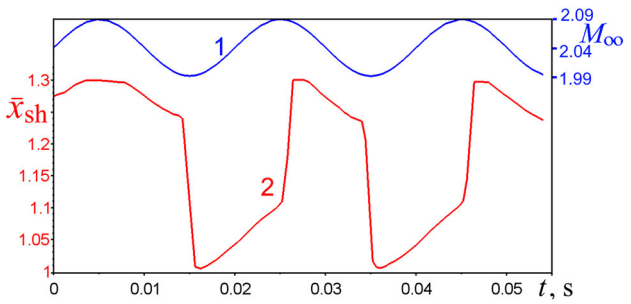

Fig. 6 1—given oscillations of M_∞; 2—calculated shock coordinate $\bar{x}_{sh}$ at $M_{mid} = 2.04$, $\tau = 0.02$ s, $A = 0.05$ and initial state with a swallowed shock

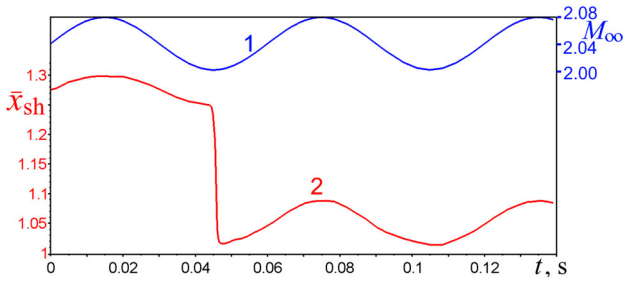

Fig. 7 1—given oscillations of M_∞; 2—calculated shock coordinate $\bar{x}_{sh}$ at $M_{mid} = 2.04$, $A = 0.04$, $\tau = 0.06$ s, which shows a transition of the shock location from the throat to the vicinity of the entrance

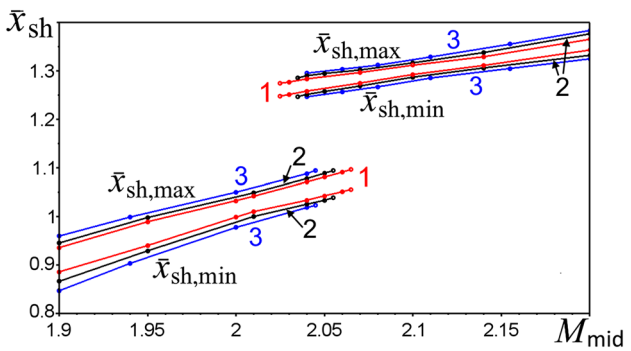

Fig. 8 Margins of the shock coordinate oscillations as functions of M_{mid} at $\tau = 0.02$ s and three amplitudes A: 1—$A = 0.02$, 2—$A = 0.03$, 3—$A = 0.04$

Meanwhile, the same increase in τ from 0.02 to 0.06 at $M_{mid} = 2.04$, $A = 0.04$ and initial state with an expelled shock (point E in Fig. 2) shows the persistence of the regime and a merely insignificant rise in the amplitude of shock coordinate oscillations from 0.035 (see Fig. 3) to 0.037.

Figure 8 depicts the maxima $\bar{x}_{sh,max}$ and minima $\bar{x}_{sh,min}$ of the shock coordinate as functions of M_{mid} at $\tau = 0.02$ s and three amplitudes A of Mach number oscillations. It can be seen that hysteresis shrinks as A increases.

4 Conclusion

The numerical simulations of supersonic flow deceleration in the convergent-divergent intake showed shock wave hysteresis with step-by-step changes in the free-stream Mach number M_∞. The upper branch of the hysteresis curve corresponds to the flow regime with a swallowed shock, whereas the lower branch corresponds to the regime with an expelled shock. The hysteresis persists under harmonic oscillations of the given Mach number $M_\infty(t)$ if the amplitude A and period τ of oscillations are sufficiently small. The hysteresis shrinks with increasing amplitude A, and it eventually disappears when A becomes sufficiently large. At moderate amplitudes ($A \approx 0.04$), the regime with swallowed shock is less stable than the one with expelled shock, as an increase in the period τ from 0.02 to 0.06 s triggers a shock expulsion. We notice that different regimes produce different losses in the total flow pressure [14, 15]; this can influence the fuel burning in the combustor and incur fluctuations in the engine thrust.

Acknowledgements This research was performed using computational resources provided by the Computational Center of St. Petersburg State University (http://cc.spbu.ru).

Funding The work was supported by Grant No. 2304-084 from St. Petersburg State University.

Data availability The author declares that the data supporting the findings of this study are available within the paper, and any supplementary information is available from the author on reasonable request.

Declarations

Conflict of interest The author has no relevant financial or non-financial interests to disclose.

References

1. Shedon J (1999) Intake aerodynamics. Blackwell Publishing Ltd., London
2. Panchal D, Chhayani D (2021) Review paper on the unstarting of the supersonic air intake. Int J Eng Res Technol 10(12). https://www.ijert.org/review-paper-on-the-unstarting-of-the-supersonic-air-intake
3. Kusunose K, Matsushima K, Maruyama D (2011) Supersonic biplane—a review. Prog Aerosp Sci 47:53–87. https://doi.org/10.1016/j.paerosci.2010.09.003
4. Yamashita H, Kuratani N, Yonezawa M, Ogawa T, Nagai H, Asai K, Obayashi S (2013) Wind tunnel testing on start/unstart characteristics of finite supersonic biplane wing. Int J Aerosp Eng Hindawi. https://doi.org/10.1155/2013/231434. (**Article 231434**)
5. Guo S, Wang Z, Zhao Y (2014) The flow hysteresis in the supersonic curved channel. J Natl Univ Defense Technol 36(4):10–14
6. Li T (2015) Study on hysteresis phenomenon caused by back pressure in curved isolator. Master's Thesis, National University of Defense Technology, Changsha, China
7. Feng S, Chang J, Zhang Ch, Wang Y, Ma J, Bao W (2017) Experimental and numerical investigation on hysteresis characteristics and formation mechanism for a variable geometry dual-mode combustor. Aerosp Sci Technol 67:96–104. https://doi.org/10.1016/j.ast.2017.03.040
8. Feng S, Chang J, Zhang Y, Zhang Ch, Wang Y, Bao W (2017) Numerical studies for performance improvement of a variable geometry dual mode combustor by optimizing deflection angle. Aerosp Sci Technol 68:320–330. https://doi.org/10.1016/j.ast.2017.05.025
9. Das S, Prasad JK (2010) Starting characteristics of a rectangular supersonic air intake with cowl deflection. Aeronaut J 114:177–189. https://doi.org/10.1017/S0001924000003626
10. Jin Y, Sun S, Tan H, Zhang Y, Huang H (2022) Flow response hysteresis of throat regulation process of a two-dimensional mixed-compression supersonic inlet. Chin J Aeronaut 35(3):112–127. https://doi.org/10.1016/j.cja.2021.06.013
11. Tang X, Fan X, Xiong B, Chen L, Chen J (2023) Study of multiple solution phenomenon for hypersonic air inlet. Aerosp Sci Technol 136:Article 108236. https://doi.org/10.1016/j.ast.2023.108236
12. Jiao X, Chang J, Wang Zh, Yu D (2016) Hysteresis phenomenon of hypersonic inlet at high Mach number. Acta Astronaut 128:657–668. https://doi.org/10.1016/j.actaastro.2016.08.025
13. Kuzmin A (2019) Shock wave instability in a bent channel with subsonic/supersonic exit. Adv Aircr Spacecr Sci 6(1):19–30. https://doi.org/10.12989/aas.2019.6.1.019
14. Kuzmin A (2019) Non-uniqueness of transonic flow in an intake-type channel. J Phys Conf Ser 1392:Article ID 012012, 1–6. https://doi.org/10.1088/1742-6596/1392/1/012012
15. Kuzmin A (2023) Non-unique regimes of oscillatory transonic flow in bent channels. Aerosp Syst. https://doi.org/10.1007/s42401-023-00243-4
16. ANSYS Fluids (2023) Computational fluid dynamics. https://www.ansys.com/products/fluids. Accessed 18 Oct 2023
17. Tennekes H, Lumley JL (1992) A first course in turbulence (14. print. ed.). MIT Press, Cambridge
18. Menter FR (2009) Review of the shear-stress transport turbulence model experience from an industrial perspective. Int J Comput Fluid Dyn 23:305–316. https://doi.org/10.1080/10618560902773387
19. Kuzmin A, Babarykin K (2018) Supersonic flow bifurcation in twin intake models. Adv Aircr Spacecr Sci 5(4):445–458. https://doi.org/10.12989/aas.2018.5.4.445